BOHR QUADRUPOLE COLLECTIVE DYNAMICS AND THE INNER FISSION BARRIER OF SOME HEAVY EVEN–EVEN NUCLEI WITHIN THE HIGHLY TRUNCATED DIAGONALIZATION APPROACH

M. Imadalou[a,b,†], M. Rebhaoui[a,c], K. Benrabia[a], D.E. Medjadi[a]

[a]Laboratoire N-corps et Structure de la Matière
Ecole Normale Supérieure Vieux-Kouba, Algiers, Algeria
[b]Faculté des Sciences, Département de Physique, Université Saad Dahlab
Route de Soumâa, BP 270 Blida, Algeria
[c]Ecole Normale Supérieure-Bouzareah, Algiers, Algeria

(Received October 23, 2020; accepted May 8, 2021)

Low-energy collective modes of some heavy even–even deformed nuclei are described within a microscopically-based quadrupole Bohr Hamiltonian framework. Bohr's microscopic functions were computed in the Time-Dependent Hartree–Fock–Bogoliubov (TDHFB) approach at its adiabatic limit (ATDHFB) using solutions derived from the so-called Highly Truncated Diagonalization Approach (HTDA). This approach is based on the treatment of pairing correlations via the residual delta force interaction of $|T_z| = 1$, whose intensity is fitted on the rotational properties of the first 2^+ states of a reasonably sized sample of well-deformed nuclei belonging to the studied region. This approach is successfully applied to describe some spectroscopic properties and the first fission barriers of well-deformed axial nuclei in the actinide region.

DOI:10.5506/APhysPolB.52.429

1. Introduction

In a very broad range of mass number, mean-field theories are successful in describing several nuclear properties, mainly ground-state properties. To study the low-excitation energy collective properties we will use here a Bohr Collective Quadrupole Hamiltonian based upon an approximation of the Adiabatic Time Dependent Hartree–Fock–Bogolyubov (ATDHFB) approach. The underlying family of static solutions will be determined within the Highly Truncated Diagonalization Approximation (HTDA) [1, 2] which corresponds to highly truncated shell models calculation using self-consistent

† Corresponding author: imadaloum@yahoo.fr

one-body states. Compared to other approaches such as the BCS approach, the HTDA approximation has the advantage of conserving the number of particles. It is well known that during BCS calculations, one may encounter neutron- or proton-level densities near the Fermi level that are so weak that the pairing gaps are strongly depressed or even sometimes vanishing. In such cases, the violation of the particle number conservation makes the quasi-particle vacuum approximation quite unsuited and in most cases the superfluid-normal phase transition is indeed totally spurious. One may also come across some computational difficulties upon calculating adiabatic mass parameters since they involve, in principle, derivatives of the density matrix with respect to a collective variable (a dependence resulting from constrained variational calculations). The HTDA approach makes it possible to overcome these difficulties by treating on the same footing all kinds of single-particle level densities at the Fermi surface.

This study is a continuation of the previous work [3] to the extent that some parameters involved in the HTDA method, as the determination of the intensity of the residual interaction, are taken up in this work. We propose to apply this new approach, which consists of adjusting the intensity of the residual delta interaction in order to reproduce the inertial momentum of the first 2^+ state in well-deformed heavy nuclei.

One of the goals is to determine the quadrupole collective properties of some actinide nuclei: ^{232}Th, ^{234}U, ^{236}U, ^{238}Pu, ^{240}Pu, and ^{246}Cm. For this purpose, we yield microscopic solutions treating the pairing correlations within an HTDA approach where the intrinsic axial symmetry is broken. Using the Belyaev approach [4], we calculate the mass parameters and the moments of inertia to define (together with the potential energy) our Bohr Hamiltonian. However, as it is well known (see *e.g.* [5]) the Belyaev approach ignores some time-odd self-consistent contributions leading to an underestimation of the adiabatic parameters. In the case of rotations, where a comparison with Thouless–Valatin (Routhian) calculations can be made, such a correction has been evaluated as an increase of 32% [6]. For the vibrational modes now, in absence of such a measuring stick, we have assumed that the same correction should hold.

Another objective is to determine the first fission barriers of the considered nuclei. For that, the phenomenological nucleon–nucleon effective interactions of the Skyrme type with the SkM* parametrization [7] have been chosen for the particle–hole part of the interaction. Its underlying surface tension properties have been explicitly adjusted to the liquid-drop fission barrier of ^{240}Pu from the original SkM parametrization [8]. This makes it suitable for fission barrier calculations. Moreover, it has been proven to provide a very satisfactory systematic reproduction of nuclear deformation and single-particle properties (see *e.g.* [9, 10]).

2. Formalism

2.1. Microscopic part

A general scheme of the HTDA approach can be summarized as follows. We start from the Hamiltonian

$$\widehat{H} = \widehat{K} + \widehat{v}_{\mathrm{SK}}\,, \tag{1}$$

where $\widehat{K}$ is the kinetic energy and $\widehat{v}_{\mathrm{SK}}$ is the Skyrme effective interaction. We perform HF+BCS calculations with some 'reasonable' seniority force to get a good ansatz $\widehat{\rho}$ for the density matrix of the correlated solution which, in turn, defines a mean field $\widehat{V}_0 \approx \mathrm{Tr}(\widehat{\rho}\,\widehat{v}_{\mathrm{SK}})$ and the corresponding 1-body Hamiltonian $\widehat{H} = \widehat{K} + \widehat{V}_0$, and whose ground state is the Slater determinant $|\Psi_0\rangle$. The state $|\Psi_0\rangle$ is considered as a quasi-vacuum (for p–h quasi-particles) and normal products below are to be defined with respect to it. Next, we rewrite $\widehat{H}$ as [11]

$$\widehat{H} = \widehat{H}_{\mathrm{IQP}} + \widehat{v}_{\mathrm{res}} + \langle\Psi_0|\widehat{H}|\Psi_0\rangle \tag{2}$$

with $\widehat{H}_{\mathrm{IQP}} =: \widehat{H}_0 :$ and $\widehat{v}_{\mathrm{res}} =: \widehat{v}_{\mathrm{SK}} : + : \widehat{\overline{V}} - \widehat{V}_0 :$, where $\widehat{\overline{V}}$ is the 1-body reduction of $\widehat{v}_{\mathrm{SK}}$ for $|\Psi_0\rangle$.

In the next step, we make two main approximations:

1. We neglect $: \widehat{\overline{V}} - \widehat{V}_0 :$ assuming that correlations do not influence much the mean field.

2. We assume $: \widehat{v}_{\mathrm{SK}} :=: \widehat{v}_\delta :$, where $\widehat{v}_\delta$ is a spin-singlet δ-force, both for simplicity and because the p–p h–h properties of the Skyrme force in use are not reliable being not a part in its fitting process. Furthermore, we assume that it acts only for pairs with $|T_z| = 1$, *i.e.* neutron–proton pairing is ignored which is a very safe approximation for nuclei far enough, as it is the case here, from the $N = Z$ line.

The strength of the δ interaction in the HTDA approach has been determined by equalling the moment of inertia provided in the Inglis–Belyaev standard expression [4] and corrected for the missing Thouless–Valatin terms as discussed above (with usual notations)

$$J_k^{\mathrm{IB}} = \hbar^2 \sum_{\mu\nu} \frac{\left|\langle\mu|\widehat{I}_k|\nu\rangle\right|^2}{(E_\mu + E_\nu)} \left(u_\mu v_\nu - u_\nu v_\mu\right)^2 \tag{3}$$

to the experimental moment of the first 2^+ state, given as it is usually done by $J_1^{\mathrm{exp}} = 4\hbar^2/(E_{4^+} - 2E_{2^+})$, where E_{4^+} and E_{2^+} are the experimental energies of the two first excited states of the ground-state band [12–17].

Finally, we diagonalize $\widehat{H}$ separately for protons and neutrons in a basis composed of one, two and three 'Cooper' pairs for both charge states, *i.e.* we determine the following factorized HTDA solution $|\Psi_n\rangle|\Psi_p\rangle$.

In order to describe general quadrupole excitation, we need to construct correlated wave functions $|\Psi\rangle$ corresponding to various triaxial shapes of a nucleus or, more precisely, characterized by various values of components of the quadrupole mass tensor. This is achieved by using constraints on the mean value of two non-vanishing components of the quadrupole operator

$$\begin{aligned} q_0 &= \left\langle \widehat{Q}_{20} \right\rangle = \left\langle \sum_{i=1}^{A} \left(3z_i^2 - r_i^2\right) \right\rangle , \\ q_2 &= \left\langle \widehat{Q}_{22} \right\rangle = \left\langle \sum_{i=1}^{A} \left(x_i^2 - y_i^2\right) \right\rangle . \end{aligned} \tag{4}$$

The calculations are performed using an expansion of the single-particle states entering $|\Psi_0\rangle$ and $|\Psi\rangle$ in an appropriate basis [18].

2.2. Collective Hamiltonian in five dimensions

We used the general Bohr Hamiltonian to describe low-energy states, depending on a complete set of quadrupole collective coordinates that describe the surface of a deformed nucleus

$$R = R_0 \left(1 + \sum_{\mu=-2}^{2} \alpha_\mu Y_{2\mu}^* \right) . \tag{5}$$

These coordinates are to be set in terms of β and γ parameters and (ϕ, θ, ψ) Euler angles. The angles $(\phi, \theta, \psi) \equiv \Omega$ define the orientations of the intrinsic principal axes in the laboratory frame

$$\alpha_\mu = D_{\mu 0}^2(\Omega)\beta\cos\gamma + \frac{1}{\sqrt{2}}\left[D_{\mu 2}^2(\Omega) + D_{\mu -2}^2(\Omega)\right]\beta\sin\gamma , \tag{6}$$

where $D_{\mu\nu}^\lambda$ is the Wigner function [19]. We can write the general Bohr Hamiltonian in the following form:

$$H = T_{\text{vib}} + T_{\text{rot}} + V , \tag{7}$$

where

$$\begin{aligned} T_{\text{vib}} = -\frac{\hbar^2}{2\sqrt{wr}} \Bigg\{ & \frac{1}{\beta^4} \left[\partial_\beta \left(\beta^4 \sqrt{\frac{r}{w}} B_{\gamma\gamma} \partial_\beta \right) - \partial_\beta \left(\beta^3 \sqrt{\frac{r}{w}} B_{\beta\gamma} \partial_\gamma \right) \right] \\ & + \frac{1}{\beta \sin 3\gamma} \left[- \partial_\gamma \left(\sqrt{\frac{r}{w}} \sin 3\gamma B_{\beta\gamma} \partial_\beta \right) + \frac{1}{\beta} \partial_\gamma \left(\sqrt{\frac{r}{w}} \sin 3\gamma B_{\beta\beta} \partial_\gamma \right) \right] \Bigg\} , \end{aligned} \tag{8}$$

$$T_{\rm rot} = \frac{1}{2}\sum_{k=1}^{3}\frac{I_k^2}{J_k}\,, \qquad J_k = 4\beta^2 B_k \sin^2\left(\gamma - \frac{2}{3}k\pi\right)\,, \tag{9}$$

$$V = V_{\rm coll}(\beta,\gamma)\,. \tag{10}$$

The intrinsic components of total angular momentum are denoted as I_k ($k = 1,2,3$), while w and r are the determinants of the vibrational and rotational tensors

$$w = B_{\beta\beta}B_{\gamma\gamma} - B_{\beta\gamma}^2\,, \qquad r = B_1 B_2 B_3\,. \tag{11}$$

The volume element which ensures the Hermiticity of $\widehat{H}$ has the form of $\mathrm{d}\tau = \sqrt{wr}\mathrm{d}\tau_0$, where $\mathrm{d}\tau_0 = \beta^4|\sin(3\gamma)|\mathrm{d}\beta\mathrm{d}\gamma\mathrm{d}\Omega$ is the standard five-dimensional harmonic oscillator volume element.

In our approximate version of the ATDHFB method (within the so-called Belyaev cranking approximation in its so-called $M(Q)$ version, see Ref. [5]), the vibrational mass parameters with respect to q_0, q_2 variables are given by

$$B_{kj} = \frac{\hbar^2}{2}\left(\mathcal{M}_{(1)}^{-1}\mathcal{M}_{(3)}\mathcal{M}_{(1)}^{-1}\right)_{kj}\,, \qquad k,j = 0,2$$

$$\mathcal{M}_{(n),kj} = \sum_{\mu,\nu}\frac{\langle\mu|\widehat{Q}_{2k}|\nu\rangle\langle\nu|\widehat{Q}_{2j}|\mu\rangle}{(E_\mu + E_\nu)^n}(u_\mu v_\nu + u_\nu v_\mu)^2\,, \tag{12}$$

where $\widehat{Q}_{2k}$ stands for one of the two quadrupole operators, $\widehat{Q}_{20}$ and $\widehat{Q}_{22}$. Instead of q_0, q_2, we often use dimensionless deformation β,γ variables

$$\beta\cos\gamma = Dq_0\,, \qquad \beta\sin\gamma = \sqrt{3}Dq_2\,, \qquad D = \sqrt{\frac{\pi}{5}}\frac{1}{A\overline{r^2}} \tag{13}$$

using the liquid drop estimate $\overline{r^2} = \frac{3}{5}(r_0 A^{1/3})^2$, $r_0 = 1.2$ fm. Note also that the determination of equivalent quasi-particle energy from our HTDA solution has been discussed in Ref. [20].

The collective potential energy is defined in the ATDHFB method as

$$V_{\rm coll} = \langle\Psi|\widehat{H}|\Psi\rangle\,. \tag{14}$$

The B_{kj} mass parameters are readily transformed into those associated with the β,γ variables. Together with the potential energy and the moments of inertia, they define our Bohr Hamiltonian [21, 22]. An expansion of eigenfunctions in terms of the base functions that depend on the deformation variables β and γ and the Euler angles ϕ,θ, and ψ [23–26] are used by the methods to solve the eigenvalue problem of general collective Hamiltonian Eq. (7). The main task is the construction of an appropriate basis

for each value of the angular-momentum quantum number where the eigenvalue problem is reduced to a simple matrix diagonalization. We construct basic states applying the second approach according to the method described in [6, 26–29]. We choose a complete set of square integrable functions

$$\Phi^{IM}_{Lmn}(\beta,\gamma,\Omega) = \mathrm{e}^{\frac{-\mu^2\beta^2}{2}}\beta^n \left\{ \begin{array}{c} \cos m\gamma \\ \sin m\gamma \end{array} \right\} D^{I^*}_{MK}(\Omega)\,. \tag{15}$$

The angular momentum: $L = -I, \ldots, I$ determines the projections of M, L. The parameter n may take any integer value which is not negative, whereas in the calculations in hand, a certain cut-off value $n_{\max}$ has to be imposed. The allowed values of m are $m = n, n-2, \ldots, 0$ or 1. By the choice of the functions $\mathrm{e}^{\frac{-\mu^2\beta^2}{2}}$, we ensure that the basis states generate wave functions that vanish at large deformations ($\beta \to \infty$). We need to adjust the basis parameter μ for each nucleus. For a broad range of values of the parameter μ, we can find a stable ground-state solution of the cut-off value $n_{\max}$ that is large enough. Certain symmetry conditions are to be fulfilled by the basis states. These conditions are originated from the fact that the choice of the body-fixed frame is not unique. Under laboratory conditions and for a given quadrupole tensor α_μ, we have 24 possible orientations of the body-fixed right-hand coordinate system that correspond to a variety of values of the variables β, γ and Ω. This basis state in the body-fixed frame must be invariant with respect to the transformations. These transformations connect various choices of the body-fixed frame. A finite group isomorphic to the octahedral point group O [30, 34] is formed by the previous transformations. A linear combinations of the states (15) fulfil this symmetry condition

$$\xi^{IM}_{Lmn}(\beta,\gamma,\Omega) = \mathrm{e}^{\frac{-\mu^2\beta^2}{2}}\beta^n \sum_{K\in\Delta I} f^I_{LmK}(\gamma)\Phi^I_{MK}(\Omega)\,. \tag{16}$$

The angular part corresponds to linear combinations of the Wigner functions

$$\Phi^I_{MK}(\Omega) = \sqrt{\frac{2I+1}{16\pi^2(1+\delta_{K0})}}\left[\mathcal{D}^{I^*}_{MK}(\Omega) + (-1)^I\mathcal{D}^{I^*}_{M-K}(\Omega)\right]. \tag{17}$$

This wave function must not depend on a choice of the intrinsic axes, *i.e.* it must be invariant under the octahedral group. The summation in Eq. (16) is over the allowed set of the K values

$$\Delta I = \left\{ \begin{array}{ll} 0, 2, ..., I & \text{for } I = 0 \pmod 2 \\ 2, 4, ..., I-1 & \text{for } I = 1 \pmod 2 \end{array} \right. . \tag{18}$$

We can use the over-complete basis set Eq. (16) to select linearly-independent functions for the next step to enforce the correct behaviour of solutions on

the $\gamma = n\frac{\pi}{3}$ axes [30]. We need to discard some of the basis states which are not orthogonal. Even though the Hamiltonian can also be diagonalized directly in a non-orthogonal basis [25], we use the Cholesky–Banachiewicz method to orthogonalize the basis states [35] The diagonalization of the collective Hamiltonian yields the energy spectrum E^I_α and the corresponding eigenfunctions

$$\Psi^{IM}_\alpha(\alpha,\beta,\Omega) = \sum_{K\in\Delta I} \psi^I_{\alpha,K}(\beta,\gamma)\Phi^I_{MK}(\Omega)\,. \tag{19}$$

The density of probability in collective space writes

$$\rho^{I,\alpha}(\beta,\gamma) = \sum_{K\,\text{even}\geq 0} \left|\psi^I_{\alpha,K}(\beta,\gamma)\right|^2 \mu(\beta,\gamma)\,, \tag{20}$$

where $\psi^I_{\alpha,K}(\beta,\gamma)$ are the collective wave functions and μ is the metric involving moments of inertia and mass parameters, in such a way that for the normalized state, one has

$$\mu(\beta,\gamma) = \left[\left(B_{00}B_{22} - B^2_{02}\right)\prod_{k=1}^{3} J_k\right]^{\frac{1}{2}}. \tag{21}$$

The reduced E2 transition probability between an initial (α, I) and a final (α', I') state of our spectrum writes

$$B\left(\text{E2};(\alpha,I)\longrightarrow(\alpha',I')\right) = \frac{1}{2I+1}\left|\langle\alpha' I'\|\hat{\mathcal{M}}(\text{E2})\|\alpha I\rangle\right|^2, \tag{22}$$

and the spectroscopic quadrupole moment of the state $|\alpha I\rangle$ is

$$Q^{\text{spec}}_{\alpha I} = \frac{1}{2I+1}C^{II}_{II20}\langle\alpha I\|\hat{\mathcal{M}}(\text{E2})\|\alpha I\rangle\,, \tag{23}$$

where $\hat{\mathcal{M}}(\text{E2})$ stands for the electric quadrupole operator. Reference [30] gives detailed expressions for the reduced matrix element $\langle\alpha' I'\|\hat{\mathcal{M}}(\text{E2})\|\alpha I\rangle$.

3. Results

3.1. Salient numerical aspects

The rapid convergence of the HTDA method depends crucially on the quality of the quasi-particle vacuum on which the many-body basis states are constructed [1, 11]. For that, HTDA calculations are initiated from the solutions of self-consistent Hartree–Fock plus BCS calculations using the

Skyrme SkM* effective interaction. The BCS calculations have been performed for single-particle states corresponding to all canonical basis whose single-particle energy is less than $\lambda_q + 6$ MeV, where λ_q is the Fermi level for the charge state q. The seniority G force matrix elements g_q depend smoothly on the number N_q of nucleons of charge q as

$$g_q = \frac{G_q}{11 + N_q}\,. \tag{24}$$

The values of the parameters have been taken from Ref. [31], where one has found the optimal set $G_n = G_p = 16$ MeV. This set yields a very satisfactory reproduction of the above-discussed odd–even mass differences for the isotopes considered in this study. Also, this intensity gave good results for the first fission barrier calculations by the BCS approach of nuclei in the actinide region (see Ref. [32]).

The canonical basis states have been projected on a truncated basis of the axially-symmetric harmonic oscillator. In practice, the basis set must, of course, be truncated. It has been done upon using the deformation-dependent prescription of Ref. [33]

$$\hbar\omega_\perp(n_\perp + 1) + \hbar\omega_z\left(n_z + \frac{1}{2}\right) \leq \hbar\omega_0(N_0 + 2)\,. \tag{25}$$

We have chosen $N_0 = 16$. It is a reasonable compromise between accuracy and feasibility to describe the whole fission barriers of actinide nuclei (see Ref. [9]). Usual axial harmonic oscillator parameters $b = \sqrt{m\omega_0/\hbar}$ and $q = \omega_\perp/\omega_z$, where m is the nucleon mass, are optimized on a regular mesh of solutions obtained on the axial edges of the (β, γ) sextant and linearly interpolated at constant β values with respect to the $\cos 3\gamma$ invariant (see *e.g.* Ref. [10] for details). Numerical integrations were made using a Gauss–Laguerre and Gauss–Hermite approximation scheme with, respectively, 18 and 50 mesh points.

As explained above, we take stock of the BCS solutions to initiate our HTDA calculations through the corresponding mean fields $\widehat{V}_0$. The same SkM* interaction is used in the Hartree–Fock part of the HTDA calculations as in the BCS approximation. The pairing correlations are treated in our HTDA approach with a residual delta force interaction form zero range ($S = 0$, $T = 1$) without density dependence, where the strength V_0 of this interaction (identical for both charge states) is obtained by following the procedure described in Ref. [3] for the actinide regions. We obtain $V_0 = -586$ MeV fm^3.

In practical HTDA applications, as in any shell-model calculations, the many-body basis in which the Hamiltonian is diagonalized has to be truncated. In our case, the many-body basis has been defined by considering

only canonical basis states lying in a band of ±5 MeV around the proton and neutron Fermi energies corresponding to $|\Psi_0\rangle$. From them, we define a model space including single-pair, double-pair and triple-pair excitations with respect to the quasi-vacuum $|\Psi_0\rangle$. Such a many-body basis supplemented by the vacuum being established, we proceed to the diagonalization of the HTDA Hamiltonian.

3.2. Potential energy surfaces

In order to determine the static deformation variables $(\beta_{\rm eq}, \gamma_{\rm eq})$ and deformation energies of the considered nuclei, we have performed HTDA calculations by imposing constraints on the expectation values of the quadrupole moments $\langle\widehat{Q}_{20}\rangle$ and $\langle\widehat{Q}_{22}\rangle$ (*cf.* Eq. (4)). They are self-consistent for actinide nuclei and so far only perturbative (from the ansatz $|\Psi_0\rangle$), for 222 points forming a regular grid in the sextant defined by $0 \leq \beta \leq 0.85$, $0 \leq \gamma \leq 60^\circ$, corresponding to mesh sizes of 0.05 and 5° in the β and γ direction, respectively.

In Fig. 1, we display the self-consistent HTDA triaxial quadrupole binding energy maps of all considered nuclei in the β–γ plane. All energies are normalized with respect to the binding energy of the absolute minimum. The equilibrium solutions corresponding to the deformation parameters $(\beta_{\rm eq}, \gamma_{\rm eq})$ are displayed as black dots. They correspond to axially-symmetrical solutions for all considered nuclei, more precisely having a prolate shape, as it is apparent in the insets in Fig. 1, where we plot the self-consistent HTDA binding energy curves for the axially-symmetric configuration as functions of the deformation parameter β. Negative values of β correspond to the $\beta > 0$, $\gamma = 180^\circ$ axis on the β–γ plane. We summarize in Table I some calculated static (*i.e.* without taking into account vibrational correlations) properties. The energy of the solutions are reported for the sake of com-

TABLE I

Experimental [36] and calculated β deformation parameter values and binding energies (with obvious notation) for the six considered nuclei.

Nucleus	$\beta_{\rm st}$	$\beta_{\rm exp}$	$E_{\rm GS}$ [MeV]	$E_{\rm exp}$ [MeV]
^{232}Th	0.25	0.25	−1764.03	−1766.69
^{234}U	0.25	0.25	−1774.67	−1778.57
^{236}U	0.26	0.27	−1786.95	−1790.42
^{238}Pu	0.30	0.30	−1796.04	−1801.27
^{240}Pu	0.30	0.30	−1809.03	−1813.45
^{246}Cm	0.30	0.29	−1842.80	−1847.83

pleteness, they have nevertheless to be decreased by the truncation energy correction as well as by the amount of spurious rotational energy. The total correction is deemed to be of the order of magnitude of the discrepancy between calculated and experimental masses [36].

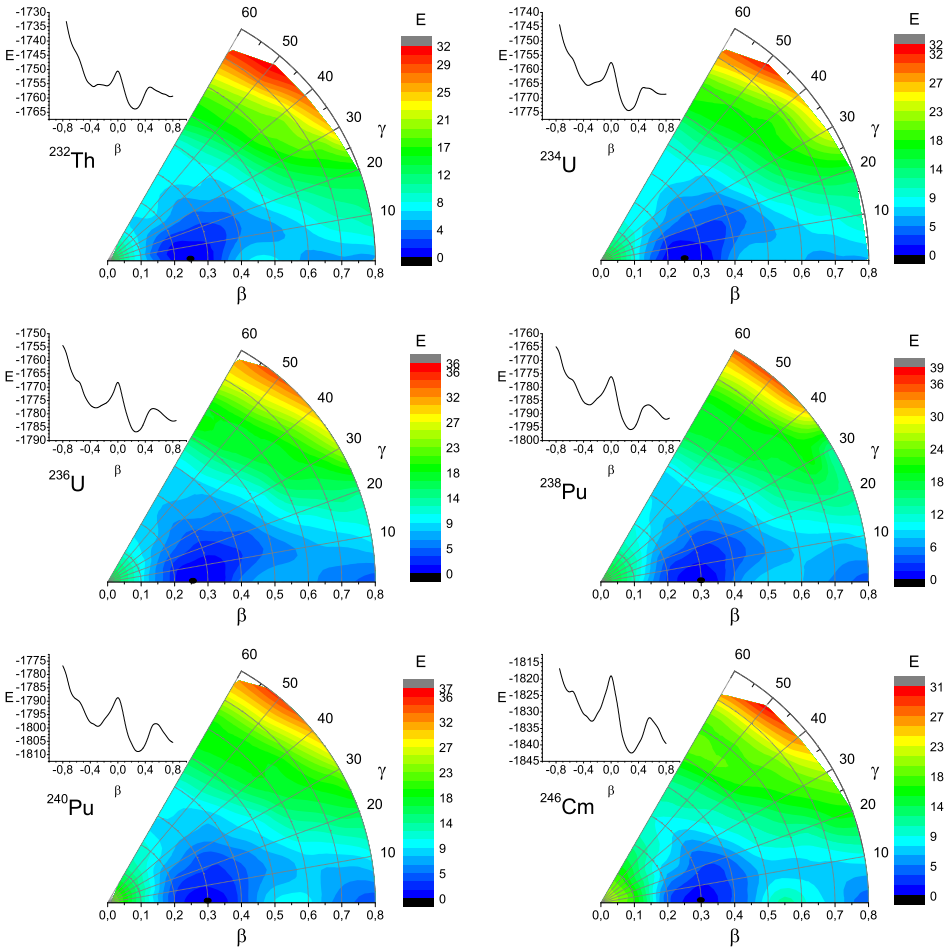

Fig. 1. Potential energy surfaces as functions of the (β, γ) variables for the six considered nuclei. In the upper-left panels, the potential energy curves of the axial solutions are reported as functions of the axial deformation parameter β. Energies are given in MeV.

3.3. Collective spectra

The calculated energy spectra are compared with experimental data [12–17]. The energy levels are grouped into the ground state, quasi-β and quasi-γ bands. As shown in Fig. 2, the corresponding calculated ground-state bands

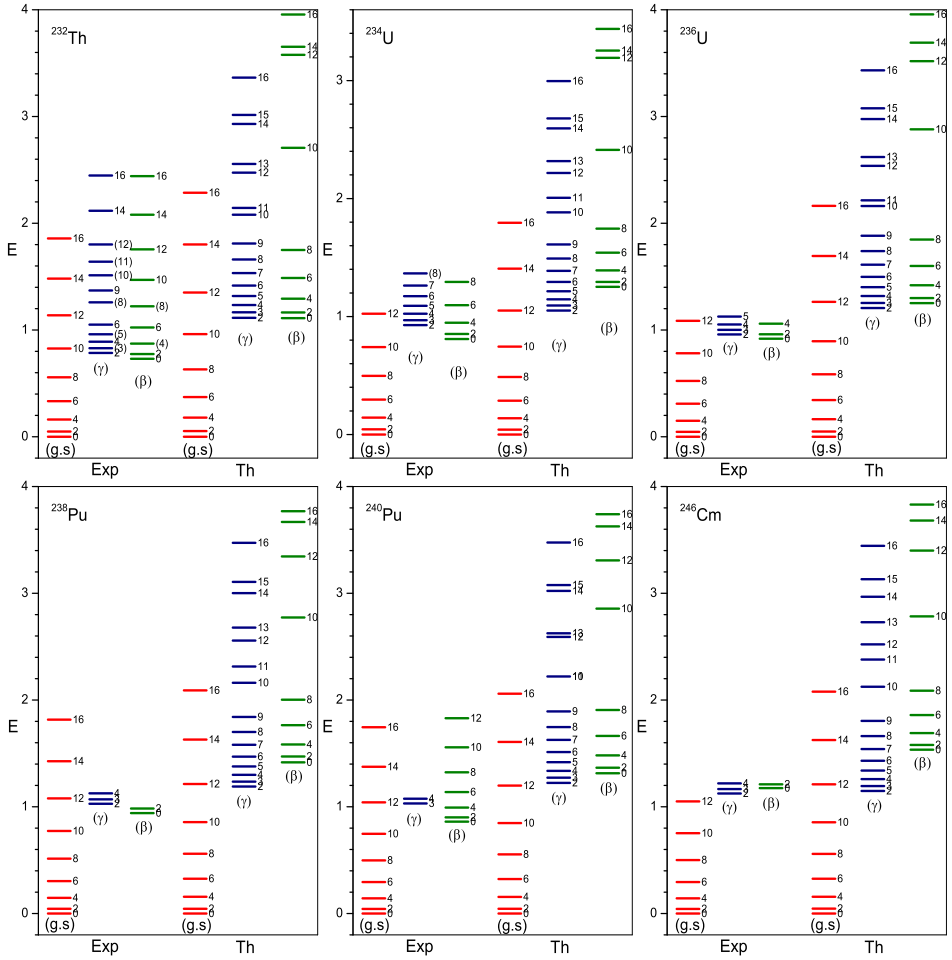

Fig. 2. Experimental and calculated (HTDA+Bohr) low-energy spectra in considered nuclei. The experimental spectra are taken from Refs. [12–17]. Energies are given in MeV.

are in reasonably good agreement with the available data in actinide nuclei of our sample. This is the result of the adjustment process that was performed to determine the strength of the residual interaction, in order to obtain adiabatic moments of inertia comparable to the experimental data. This concordance between computational and experimental energy levels in quasi-β and quasi-γ bands gets worse as kinetic moment increases. This is simply explained by the fact that the moments of inertia are computed in the adiabatic limit, but are used in highly non-adiabatic instances when the value of I is large. As a result, we obtain phonon energies that are too high

for degrees of freedom β and γ, as it is apparent on the two upper panels of Fig. 3. This provides another indication of the absence of rotation–vibration coupling for these states.

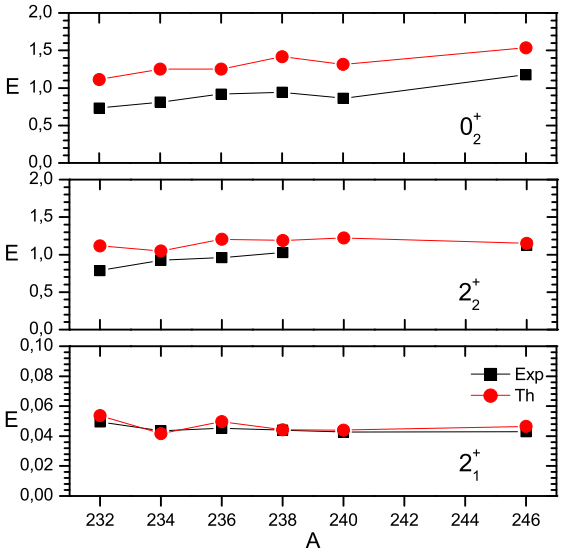

Fig. 3. Excitation energies (in MeV) of the first and second 2^+ states and second 0^+ state as functions of the considered nuclei referred to by their particle number A. Theoretical values calculated within the HTDA+Bohr approach are compared with experimental data [12–17].

To estimate quantitatively the difference between the calculated and experimental values in vibrational bands, we have presented in Figs. 4 and 5, the gaps $\Delta E(I)$ between consecutive energy levels in the ground state, quasi-β and quasi-γ bands, respectively, for the ^{232}Th and ^{240}Pu nuclei. The other considered nuclei do not present sufficient experimental data in vibrational bands for a comparison. As can be seen in these figures, the theoretical curves of the differences between energy levels of the ground-state bands are regular and have the same shape as the experimental one. This indicates, that the ground-state bands are well reproduced. This agreement between the calculated and experimental values deteriorates in quasi-β and quasi-γ bands, where irregularities appear clearly for states greater than 8^+ in the β-band and states greater than 9^+ in the γ-band. In particular, for the two considered nuclei, the average gap between the 10^+ and 8^+ states in the β-band is very high, it is worth 3.17 times the experimental one and that between 12^+ and 10^+ states is 2.36 times the experimental, while for the ^{232}Th nucleus, the gaps between the 10^+ and 9^+ states and that between 12^+ and 11^+ states of the γ-band are, respectively, 1.70 and 1.87 times the experimental gap.

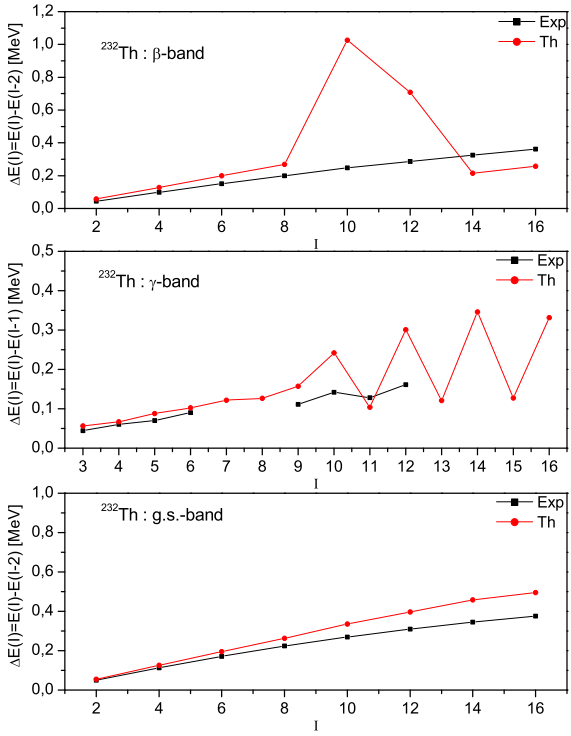

Fig. 4. The theoretical and experimental gaps $\Delta E(I)$ between consecutive energy levels in the ground-state band, β-band and γ-band for the ^{232}Th nucleus.

3.4. Transition probabilities and spectroscopic quadrupole moments

It is well known that the use of microscopic models based on a self-consistent mean-field single-particle solution is well suited for calculating physical observables, such as transition probabilities and quadrupolar spectroscopic moments in the configuration space. The transition probabilities between eigenvectors of the collective Hamiltonian, using the value of the proton charge in the electric quadrupole operator $\hat{\mathcal{M}}(\mathrm{E2})$, can be compared with data in a direct way. In Fig. 6, we compared the resulting values $B(\mathrm{E2})$ for the transitions from the first state 2^+ to the ground state 0^+ with the experimental values available for all the nuclei considered. We have a good agreement between the theoretical values and the experimental data except for the two isotopes of Pu which present slightly higher transitions. This is a good indication when reproducing the quadrupole deformation of the collective wave function. Such an agreement has been already obtained at the static HTDA level but its confirmation here is another proof of the rigidly deformed character of our solution. Spectroscopic charge quadrupole mo-

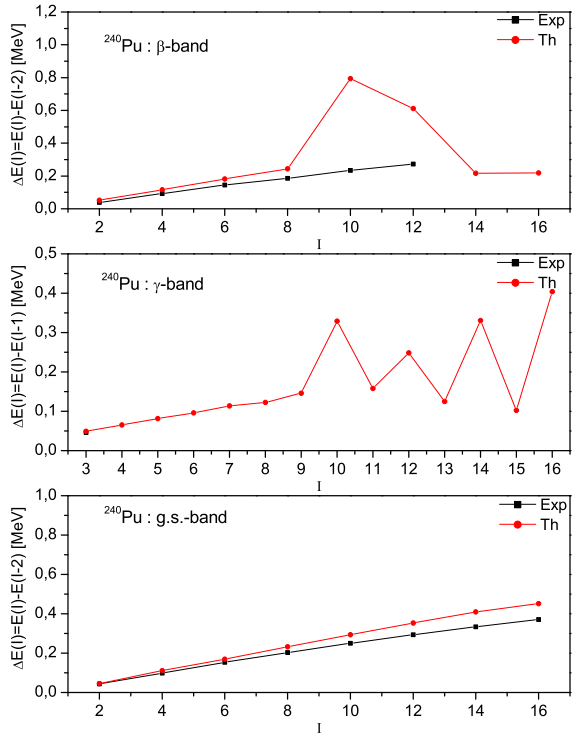

Fig. 5. The theoretical and experimental gaps $\Delta E(I)$ between consecutive energy levels in the ground-state band, β-band and γ-band for the ^{240}Pu nucleus.

ments calculated from the first 2^+ state wave functions may be transformed into intrinsic charge quadrupole moments for well (axially) deformed nuclei within the Bohr–Mottelson rotor model according to

$$\left\langle \widehat{Q}^{\mathrm{p}}_{20} \right\rangle = Q^{\mathrm{p}}_{\mathrm{sp}}(I,K)\frac{(I+1)(2I+3)}{3K^2 - I(I+1)}\,, \tag{26}$$

where $\hbar K$ is the projection on the quantization axis of the total nuclear angular momentum. For the first 2^+ state where $K=0$ and $I=2$, one has $\langle \widehat{Q}^{\mathrm{p}}_{20} \rangle = -7Q^{\mathrm{p}}_{\mathrm{sp}}/2$. Such HTDA intrinsic quadrupole moments are shown in Fig. 7 to be in rather good agreement with corresponding quantities deduced from B(E2) data [12–17]. Finally, the good agreement between data and both static HTDA and dynamical HTDA+Bohr results, as far as the (axial) intrinsic quadrupole deformation is concerned, is illustrated in Fig. 7 in another way, where corresponding Q^{p}_{20} moment values for the ground states of the studied nuclei are reported.

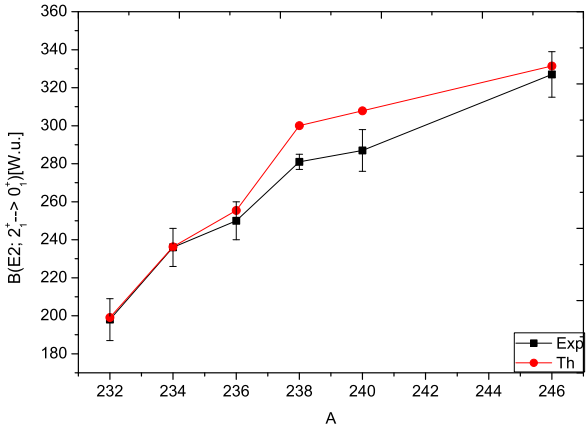

Fig. 6. Reduced transition probability $B(\mathrm{E2})$ values (in Weisskopf units) for the ground-state transitions ($2_1^+ \to 0_1^+$). Theoretical values calculated with the HTDA+Bohr approach are compared with data [12–17].

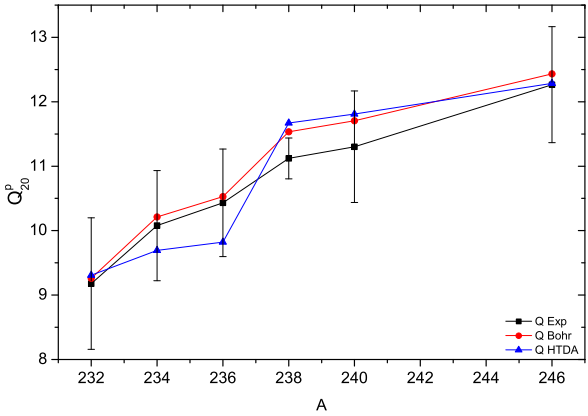

Fig. 7. Intrinsic quadrupole moments (in barns) for the six considered nuclei referred to by their particle number A. Theoretical HTDA and HTDA+Bohr results are compared with experimental data from Refs. [12–17] (squares).

3.5. Inner barrier heights

Starting from the results of axially-symmetrical HTDA calculations, we evaluate the inner barrier heights by adding various corrections. First, we have assumed that for all the considered nuclei, the basis size is sufficient to obtain the convergence of the energy difference between the ground state and the axial inner barrier solutions. This takes stock of the results of [9] for the ^{252}Cf nucleus obtained with the same Skyrme force and almost the same seniority force parametrization (see Table I in Ref. [9]).

As we know, the use of the Slater approximation for the treatment of the Coulomb exchange contribution to the total energy and the Hartree–Fock mean field yields an underestimation of the inner barrier. It is found to be given by $\Delta E^{\text{Slater}} = 310$ KeV in the ^{238}U nucleus [37]. Owing to the systematic character of such an underestimation, as discussed in [37], and to the numerically heavy character of such exact Coulomb exchange calculations, we have simply assumed here that it takes the same value for the six nuclei under study. The second correction provided is the spurious rotational energy correction. This has been approximately corrected here, within a Lipkin ansatz [38], assuming thus a perfect rotational character for the rotational band which would be obtained when projecting, namely

$$E_{\text{rot}} = \frac{\left\langle \widehat{J}^2 \right\rangle}{2I}\,, \tag{27}$$

where I is a moment of inertia. In the frame of the rigid-rotation assumption, I is constant with J. It may thus be evaluated, in particular, in the adiabatic limit of the Thouless–Valatin (Routhian) formalism. Thus, we approximate the moment of inertia I, up to self-consistent time-odd terms in the Hartree–Fock and pairing fields, by the Inglis–Belyaev moments $\mathcal{I}_{\text{Bel}}$

$$\mathcal{I}_{\text{Bel}} = \sum_{k,l}^{(1)} \frac{\left|\left\langle k|\hat{J}^+|l\right\rangle\right|^2}{E_k + E_l}(u_k v_l - u_l v_k)^2 + \frac{1}{2}\sum_{k,l}^{(2)} \frac{\left|\left\langle k|\hat{J}^+|\bar{l}\right\rangle\right|^2}{E_k + E_l}(u_k v_l - u_l v_k)^2\,, \tag{28}$$

where the first sum, labelled (1), is performed on the members of all Kramers degenerate pairs of canonical basis states, while the second sum, labelled (2), is restricted to states such that $|K_l| = |K_k| = 1/2$ (where K is the third component of the one-body angular momentum operator $\hat{j}_z$). As discussed above, the contribution of the time-odd fields can be taken care of upon multiplying the Inglis–Belyaev moments by an appropriate factor depending on the effective force used. Therefore, the total energy of the 0^+ state is approximately related to the intrinsic energy by

$$E = E_{\text{intr}} - E_{\text{rot}}\,. \tag{29}$$

We have chosen to compute both the moment of inertia $\mathcal{I}_{\text{Bel}}$ and $\langle \widehat{J}^2 \rangle$ in a consistent way. This has been achieved using axially solutions derived from the HTDA approximation. Moreover, we have assumed that for all the considered nuclei, the basis size is sufficient to obtain the convergence of the energy difference between the ground state and the axial inner barrier solutions. The spurious rotational energy correction ΔE^{rot} for an even–even

fissioning nucleus with $I^\pi = 0^+$ has been evaluated as a rotational energy difference between the ground state and the axial inner barrier solutions. As seen in Table II, it lowers the inner barrier height by about half a MeV. As shown in Table III, adding these corrections one obtains inner barrier heights $E_{\rm IB}^{\rm axial}$ which are significantly too high with respect to experimental estimates when axial symmetry is imposed. This leaves room for a decrease due to the release of the axial symmetry constraint as discussed now.

TABLE II

Rotational energies (in MeV) at the ground-state deformation ($E_{\rm GS}^{\rm rot}$) and at the axial saddle point ($E_{\rm IB}^{\rm rot}$) along with the deduced rotational energy correction to the axial inner barrier ($\Delta E^{\rm rot}$).

Nucleus	$E_{\rm GS}^{\rm rot}$	$E_{\rm IB}^{\rm rot}$	$\Delta E^{\rm rot}$
^{232}Th	1.38	1.86	−0.48
^{234}U	1.40	1.87	−0.47
^{236}U	1.38	1.76	−0.38
^{238}Pu	1.48	2.04	−0.56
^{240}Pu	1.44	1.92	−0.48
^{246}Cm	1.42	1.75	−0.33

TABLE III

Inner fission barrier heights and associated corrective terms (in MeV) for the ^{232}Th, ^{234}U, ^{236}U, ^{238}Pu, ^{240}Pu and ^{246}Cm nuclei. The following quantities are listed: axially-symmetrical HTDA inner barrier heights $E_{\rm IB}^{\rm axial}$(uncorr.), rotational energy corrections $\Delta E^{\rm rot}$, Coulomb exchange corrections $\Delta E^{\rm Slater}$ [MeV]), inner barrier heights corrected for the spurious rotational energy content, assuming axial symmetry $E_{\rm IB}^{\rm axial}$(corr.), energy corrections due to the triaxiality of the solutions $\Delta E^{\rm triax}$, resulting calculated inner barrier heights $E_{\rm IB}^{\rm calc}$ and, finally, $E_{\rm IB}^{\rm exp}$ the estimated inner barrier heights from experimental data taken from Ref. [41].

Nucleus	$E_{\rm IB}^{\rm axial}$(uncorr.)	$\Delta E^{\rm rot}$	$\Delta E^{\rm Slater}$	$E_{\rm IB}^{\rm axial}$(corr.)	$\Delta E^{\rm triax}$	$E_{\rm IB}^{\rm calc}$	$E_{\rm IB}^{\rm exp}$
^{232}Th	8.27	−0.48	0.31	8.10	−2.73	5.37	5.8(3)
^{234}U	8.75	−0.47	0.31	8.59	−3.31	5.28	5.6(3)
^{236}U	9.08	−0.38	0.31	9.01	−2.36	6.65	5.6(3)
^{238}Pu	9.13	−0.56	0.31	8.88	−1.96	6.92	5.9(3)
^{240}Pu	10.19	−0.48	0.31	10.02	−3.01	7.01	5.8(3)
^{246}Cm	11.76	−0.33	0.31	11.74	−4.49	7.25	6.0(3)

However, in phenomenological studies of fission barriers [39, 40], it has been shown that the first barrier of heavy nuclei is no longer axially symmetric. Thus, the first saddle point energy is lowered when allowing triaxial shapes for the nucleus undergoing fission, while the left–right asymmetry is

not favoured at this point. More recently, in a study of the fission barriers of heavy nuclei in the region of actinides [9], it was shown, when plotting both reflection-symmetric and non-symmetric curves as a function of the axial deformation, that from the Super-Deformed minimum (second minimum) up to a particular branching point (whose abscissa depends on the considered nucleus), the left–right symmetrical shape is energetically favoured. Then, from this branching point up to far beyond the second saddle point (second fission barrier), the most stable solution becomes the asymmetric one. Furthermore, the branching point almost coincides with the top of the second asymmetric barrier, making the symmetric–asymmetric transition rather sudden. This is why we have performed deformation energy calculations around the first saddle point by considering only the quadrupolar degrees of freedom.

In order to obtain the lowest triaxial solution at a given q_0-elongation, a section in the corresponding two-dimensional potential energy surface has first to be drawn. The reeked minimum can then be roughly localized and one can perform a final calculation starting from an approximate solution by releasing the constraint on q_2. Triaxial solutions that have been obtained correspond to low values (15° at most), so that they remain rather close to symmetrical ones. Therefore, assuming that the basis parameters used for triaxial calculations should be close to those obtained in the axial calculation corresponding to the same q_0-value, we have decided to perform all triaxial calculations with the b- and q-values retained in the axial cases. The occurrence of such a symmetry breaking is illustrated in Fig. 8, where we have represented, for all studied nuclei, the sections of the potential energy surface along the q_2-direction at different q_0-elongations around the top of the first barrier. Indeed, the energetically-favoured solution appears for a non-zero q_2 value. This deformation turns out to be approximately the deformation of the barrier top for a triaxial solution Of course, the value of the axial quadrupole deformation parameter β may vary between what one obtains for the axial inner barrier solution and the triaxial one. However, these differences are small as demonstrated in Table IV. The gamma values corresponding to the triaxial saddle point are found in the 9°–15° range as seen also in Table IV. Upon releasing the axial symmetry, one lowers the inner saddle point energy by a quantity of $\Delta E_{\mathrm{IB}}^{\mathrm{triax}}$ associated with the maximal energy difference between axial and non-axial solutions

$$\Delta E_{\mathrm{IB}}^{\mathrm{triax}} = E\left(\beta_{\mathrm{IB}}^{\mathrm{triax}}, \gamma_{\mathrm{IB}}^{\mathrm{triax}}\right) - E\left(\beta_{\mathrm{IB}}^{\mathrm{axial}}, 0\right) . \tag{30}$$

The energy difference associated with the symmetry breaking amounts to roughly 2–4 MeV as can be seen in Table IV. As mentioned, the rotational correction has not been explicitly computed in the triaxial case. To take it

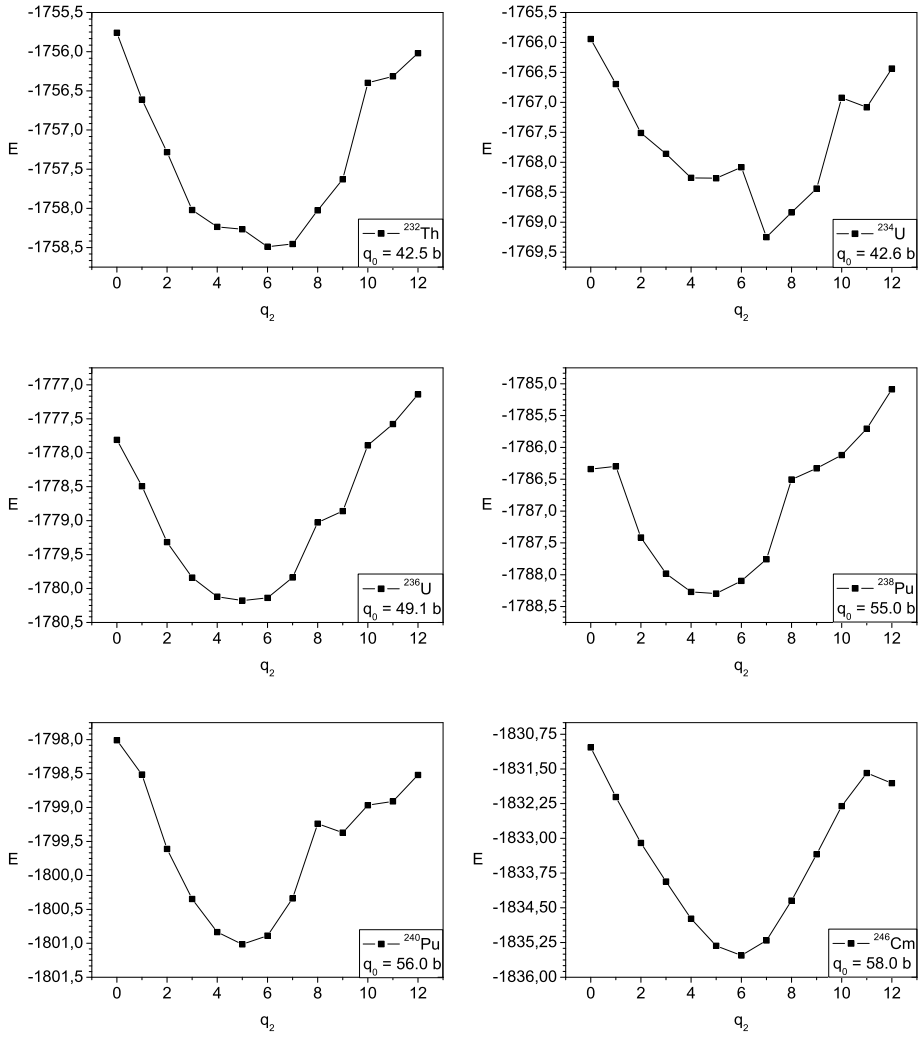

Fig. 8. Section of the potential energy surface as a function of q_2 (in barn) in the inner saddle point region for the six considered nuclei. Energies are given in MeV.

approximately into account, we have substracted from the triaxial energy the rotational energy calculated in the axial case at the same q_0-value. Finally, we add to these $E_{\mathrm{IB}}^{\mathrm{axial}}$ energies, the gain in energy $\Delta E^{\mathrm{triax}}$ obtained when considering the triaxial saddle point for the inner barrier. The resulting inner barrier height $E_{\mathrm{IB}}^{\mathrm{calc}}$ compare reasonably well with the recommended values deduced from experimental data of Ref. [41] for the first four calculated nuclei (^{232}Th, ^{234}U, ^{236}U and ^{238}Pu), it is less than 1.05 MeV. The calculated barrier heights of the last two considered nuclei (^{240}Pu and ^{246}Cm) are higher by about 1.25 MeV.

TABLE IV

Deformation parameter β values corresponding to the axial inner barrier solution ($\beta_{\mathrm{IB}}^{\mathrm{axial}}$) together with the triaxial corresponding values $\beta_{\mathrm{IB}}^{\mathrm{triax}}$ along with the associated gamma values ($\gamma_{\mathrm{IB}}^{\mathrm{triax}}$).

Nuclei	^{232}Th	^{234}U	^{236}U	^{238}Pu	^{240}Pu	^{246}Cm
$\beta_{\mathrm{IB}}^{\mathrm{axial}}$	0.45	0.44	0.50	0.55	0.55	0.55
$\beta_{\mathrm{IB}}^{\mathrm{triax}}$	0.46	0.46	0.51	0.55	0.56	0.56
$\gamma_{\mathrm{IB}}^{\mathrm{triax}}$	15.42°	15.32°	10.00°	9.07°	9.12°	10.26°

4. Conclusions

This work is the continuation of the recent article [3], in which we extended the method of determining the intensity of the residual interaction to well-deformed even–even nuclei having the axial symmetry of the actinide region.

Our HTDA calculations for solutions breaking the axial symmetry have been performed with a reputable Skyrme SkM* force parametrization and a residual interaction whose strength has been determined using a new method. These solutions have been used in the approximate version of the ATDHFB approach to determine the seven scalar functions defining the Bohr Hamiltonian, as was done in the previous cited study.

The collective spectra obtained from the diagonalization of the Bohr Hamiltonian show, for all the nuclei considered, ground-state bands in fairly good agreement with the experimental data. This agreement between the calculated and experimental energy levels deteriorates in the β-bands and γ-bands as the angular momentum increases. This is a direct consequence of the inefficiency of the adiabatic approach used here for the calculation of inertia parameters when the spin is high. This gives an indication of the absence of rotation–vibration coupling for these states. Another proof of the rigidly deformed character of our solution is the good agreement between the theoretical values and the experimental data of quadrupolar spectroscopic moments and the transition probabilities except for the two isotopes of Pu which present slightly higher transitions. As such, it provides *a posteriori* justification of the method proposed here, to adapt the strength of the residual interaction to adiabatic rotation properties of well-deformed heavy nuclei, in which the mode of rotation should be well decoupled from other collective modes.

Initially, from the HTDA axial solutions, we estimated the first fission barriers by considering the zero point rotation correction. The barrier heights thus obtained are relatively high compared to the data, but a triax-

ial calculation of these barriers allowed us to approach in a significant way experimental values. While the results of this work are already rather satisfactory, it calls nevertheless for some improvements or extensions. It would be interesting in particular to carry out these HTDA studies introducing a charge dependence of the residual delta force.

REFERENCES

[1] N. Pillet, P. Quentin, J. Libert, «Pairing correlations in an explicitly particle-number conserving approach», *Nucl. Phys. A* **697**, 141 (2002).

[2] L. Bonneau, P. Quentin, K. Sieja, «Ground-state properties of even–even $N = Z$ nuclei within the Hartree–Fock–BCS and higher Tamm–Dancoff approaches», *Phys. Rev. C* **76**, 014304 (2007).

[3] M. Rebhaoui, M. Imadalou, D.E. Medjadi, P. Quentin, «Determination of a pairing residual interaction from Bohr quadrupole collective dynamics», *J. Phys. G: Nucl. Part. Phys.* **45**, 115102 (2018).

[4] S.T. Belyaev, «Concerning the calculation of the nuclear moment of inertia», *Nucl. Phys.* **24**, 322 (1961), and references quoted therein.

[5] E.Kh. Yuldashbaeva, J. Libert, P. Quentin, M. Girod, «Mass parameters for large amplitude collective motion: A perturbative microscopic approach», *Phys. Lett. B* **461**, 1 (1999).

[6] J. Libert, M. Girod, J.P. Delaroche, «Microscopic descriptions of superdeformed bands with the Gogny force: Configuration mixing calculations in the $A \sim 190$ mass region», *Phys. Rev. C* **60**, 054301 (1999).

[7] J. Bartel *et al.*, «Towards a better parametrisation of Skyrme-like effective forces: A Critical study of the SkM force», *Nucl. Phys. A* **386**, 79 (1982).

[8] H. Krivine, O. Bohigas, J. Treiner, «Derivation of a fluid-dynamical lagrangian and electric giant resonances», *Nucl. Phys. A* **366**, 155 (1980).

[9] L. Bonneau, P. Quentin, D. Samsoen, «Fission barriers of heavy nuclei within a microscopic approach», *Eur. Phys. J. A* **21**, 391 (2004).

[10] L. Bonneau, P. Quentin, «Fission barriers and fission paths of the ^{70}Se nucleus within a microscopic approach», *Phys. Rev. C* **72**, 014311 (2005).

[11] J. Le Bloas *et al.*, «Effect of pairing correlations on the isospin-mixing parameter in deformed $N = Z$ even–even nuclei», *Phys. Rev. C* **86**, 034332 (2012).

[12] E. Browne, «Nuclear Data Sheets for $A = 232$*», *Nucl. Data Sheets* **107**, 2579 (2006).

[13] E. Browne, «Nuclear Data Sheets for $A = 234$*», *Nucl. Data Sheets* **108**, 681 (2007).

[14] E. Browne, «Nuclear Data Sheets for $A = 236$*», *Nucl. Data Sheets* **107**, 2649 (2006).

[15] F.E. Chukreev, V.E. Makarenko, M.J. Martin, «Nuclear Data Sheets for $A = 238$*», *Nucl. Data Sheets* **97**, 129 (2002).

[16] Balraj Singh, E. Browne, «Nuclear Data Sheets for $A = 240$*», *Nucl. Data Sheets* **109**, 2439 (2008).

[17] E. Browne, J.K. Tuli, «Nuclear Data Sheets for $A = 246$*», *Nucl. Data Sheets* **112**, 1833 (2011).

[18] D. Samsoen, P. Quentin, J. Bartel, «Generalized Routhian calculations within the Skyrme–Hartree–Fock approximation», *Nucl. Phys. A* **652**, 34 (1999).

[19] D.A. Varshalovich, A.N. Moskalev, V.K. Khersonskii, «Quantum Theory of Angular Momentum», *World Scientific*, 1988.

[20] M. Imadalou, D.E. Medjadi, P. Quentin, L. Prochniak, «Quadrupole collective dynamics of medium–heavy even–even nuclei within the highly truncated diagonalization approach», *Phys. Scr.* **89**, 054025 (2014).

[21] L. Próchniak, P. Quentin, D. Samsoen, J. Libert, «A self-consistent approach to the quadrupole dynamics of medium heavy nuclei», *Nucl. Phys. A* **730**, 59 (2004).

[22] L. Próchniak, S.G. Rohoziński, «Quadrupole collective states within the Bohr collective Hamiltonian», *J. Phys. G: Nucl. Part. Phys.* **36**, 123101 (2009).

[23] G.G. Dussel, D.R. Bès, «Solution of bohr's collective hamiltonian», *Nucl. Phys. A* **143**, 623 (1970).

[24] G. Gneuss, W. Greiner, «Collective potential energy surfaces and nuclear structure», *Nucl. Phys. A* **171**, 449 (1971).

[25] K. Kumar, «Lifetimes and spin-parity assignments of excited states in ^{69}Ge populated in the ^{66}Zn$(\alpha, n\gamma)$ reaction», *Nucl. Phys. A* **321**, 189 (1979).

[26] J. Libert, P. Quentin, «Self-consistent description of heavy nuclei. I. Static properties of some even nuclei», *Phys. Rev. C* **25**, 571 (1982).

[27] I. Deloncle *et al.*, «The low energy spectra of heavy transitional even nuclei from an effective nucleon-nucleon interaction», *Phys. Lett. B* **233**, 16 (1989).

[28] I. Deloncle, Ph.D. Thesis, Université de Paris 6, 1989.

[29] L. Próchniak *et al.*, «Collective quadrupole excitations in the $50 < Z$, $N < 82$ nuclei with the generalized Bohr Hamiltonian», *Nucl. Phys. A* **648**, 181 (1999).

[30] K. Kumar, M. Baranger, «Complete numerical solution of Bohr's collective Hamiltonian», *Nucl. Phys. A* **92**, 608 (1967).

[31] Meng-Hock Koh *et al.*, «Band-head spectra of low-energy single-particle excitations in some well-deformed, odd-mass heavy nuclei within a microscopic approach», *Eur. Phys. J. A* **52**, 3 (2016).

[32] K. Benrabia, D.E. Medjadi, M. Imadalou, P. Quentin, «Triaxial quadrupole dynamics and the inner fission barrier of some heavy even–even nuclei», *Phys. Rev. C* **96**, 034320 (2017).

[33] H. Flocard, P. Quentin, A.K. Kerman, D. Vautherin, «Nuclear deformation energy curves with the constrained Hartree–Fock method», *Nucl. Phys. A* **203**, 433 (1973).

[34] M. Hammermesh, «Group Theory and Its Applications to Physical Problems», *Addison-Wesley*, Reading, Massachusetts 1962.

[35] W.A. Press, B.P. Flannery, S.A. Teukolsky, W.T. Vetterling, «Numerical Recipes in C: The Art of Scientific Computing», *Cambridge University Press*, Cambridge, England 1988.

[36] From NNDC, ENSDF database, rev. Feb. 3, 2016.

[37] J. Le Bloas *et al.*, «Exact Coulomb exchange calculations in the Skyrme–Hartree–Fock–BCS framework and tests of the Slater approximation», *Phys. Rev. C* **84**, 014310 (2011).

[38] H.J. Lipkin, «Collective motion in many-particle systems», *Ann. Phys.* **9**, 272 (1960).

[39] P. Möller, J.R. Nix, Proceedings, Third IAEA Symposium on Physics and Chemistry of Fission, Rochester, 1973, Vol. I. Vienna, 1974, p. 103.

[40] V.V. Pashkevich, «The energy of non-axial deformation of heavy nuclei», *Nucl. Phys. A* **133**, 400 (1969).

[41] G.N. Smirenkin, «Preparation of evaluated data for a fission barrier parameter library for isotopes with $Z = 82$–98, with consideration of the level density models used», Technical Report No. INDC(CCP)-359, IAEA, Vienna, 1993.